Supporting Information

Zhang 10.1073/pnas.1422296112

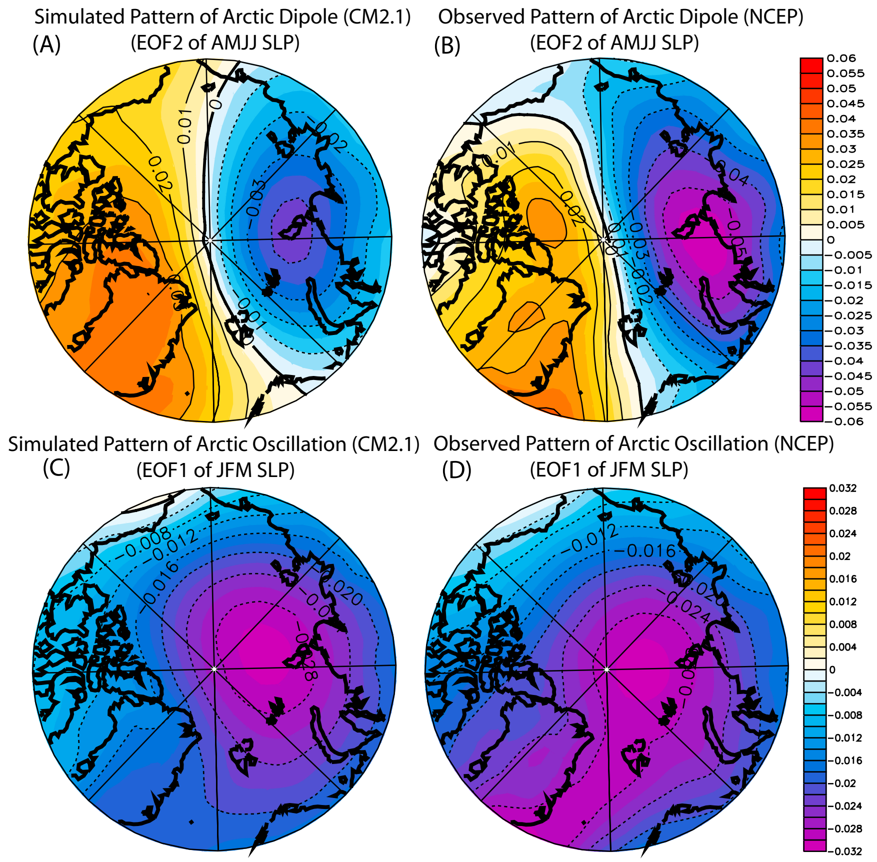

Fig. S1. Spatial patterns of simulated (3,600-y segment of CM2.1 control simulation) and observed (NCEP/NCAR reanalysis for 1948–2013) positive phases of spring AD [EOF2 of April–July (AMJJ) SLP anomaly north of Arctic Circle] and winter AO [EOF1 of January–March (JFM) SLP anomaly north of 20°N]. (*A*) Simulated AD pattern (10% of variance). (*B*) Observed AD pattern (12% of variance). The AD pattern (EOF2) is dimensionless, and the amplitude of AD is carried by the AD index (PC2). The SDs of simulated and observed unfiltered AD index are 38.5 hPa and 31.7 hPa, respectively. (*C*) Simulated AO pattern (52% of variance). (*D*) Observed AO pattern (48% of variance). The AO pattern (EOF1) is dimensionless, and the amplitude of AO is carried by the AO index (PC1). The SDs of simulated and observed unfiltered AO index are 159.7 hPa and 213.8 hPa, respectively.

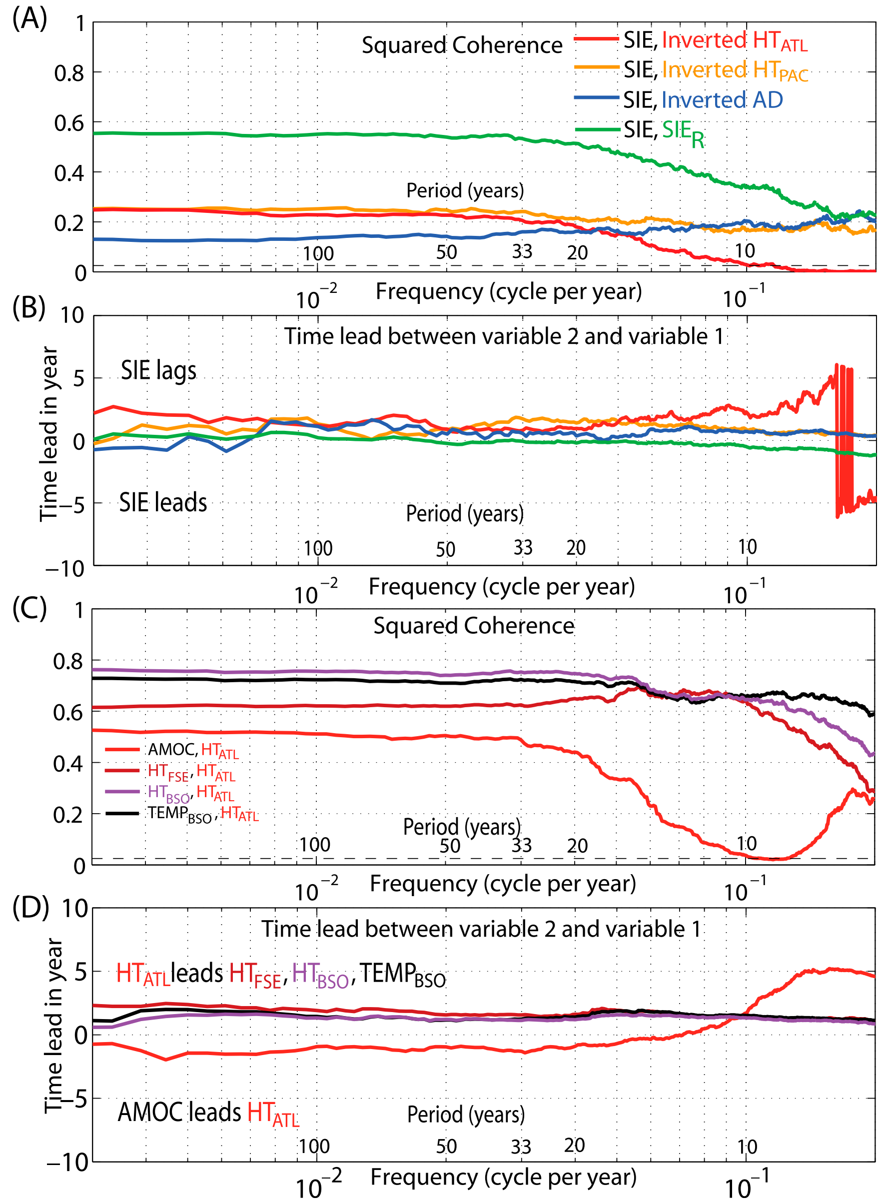

Fig. S2. Cross-spectral analysis from CM2.1. (*A* and *B*) Squared coherence (*A*) and time lead in years (*B*) among unfiltered variables (simulated September Arctic SIE anomalies vs. reconstructed September Arctic SIE anomalies, inverted HT_{ATL}, HT_{PAC}, and AD anomalies). (*C* and *D*) Squared coherence (*C*) and time lead in years (*D*) among unfiltered variables [AMOC Index vs. HT_{ATL} anomalies; HT_{ATL} anomalies vs. anomalous HT_{BSO}, HT_{FSE}, and $TEMP_{BSO}$ (averaged Atlantic Water temperature at 200 m along BSO)]. The dashed black lines in *A* and *C* are the 99% significance levels.

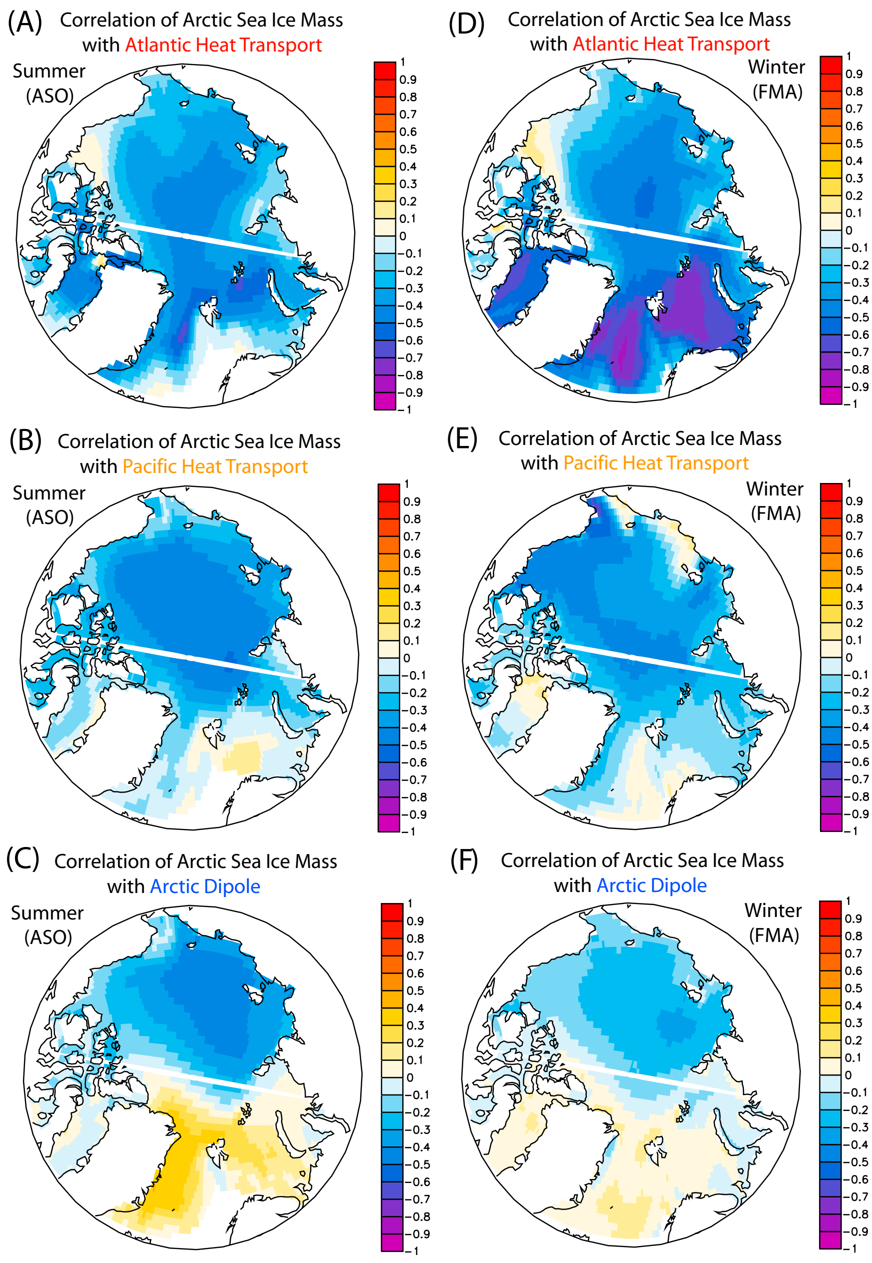

Fig. S3. Correlation maps between 30-y LF Arctic sea ice mass anomalies (kilogram per square meter) and each of the three LF predictors in CM2.1 at summer [August–October (ASO)] (*A*–*C*) and winter [February–April (FMA)] (*D*–*F*), respectively. (*A* and *D*) Correlations with anomalous HT_{ATL} (2-y lead). (*B* and *E*) Correlations with anomalous HT_{PAC} (2-y lead). (*C* and *F*) Correlations with anomalous AD (1-y lead).

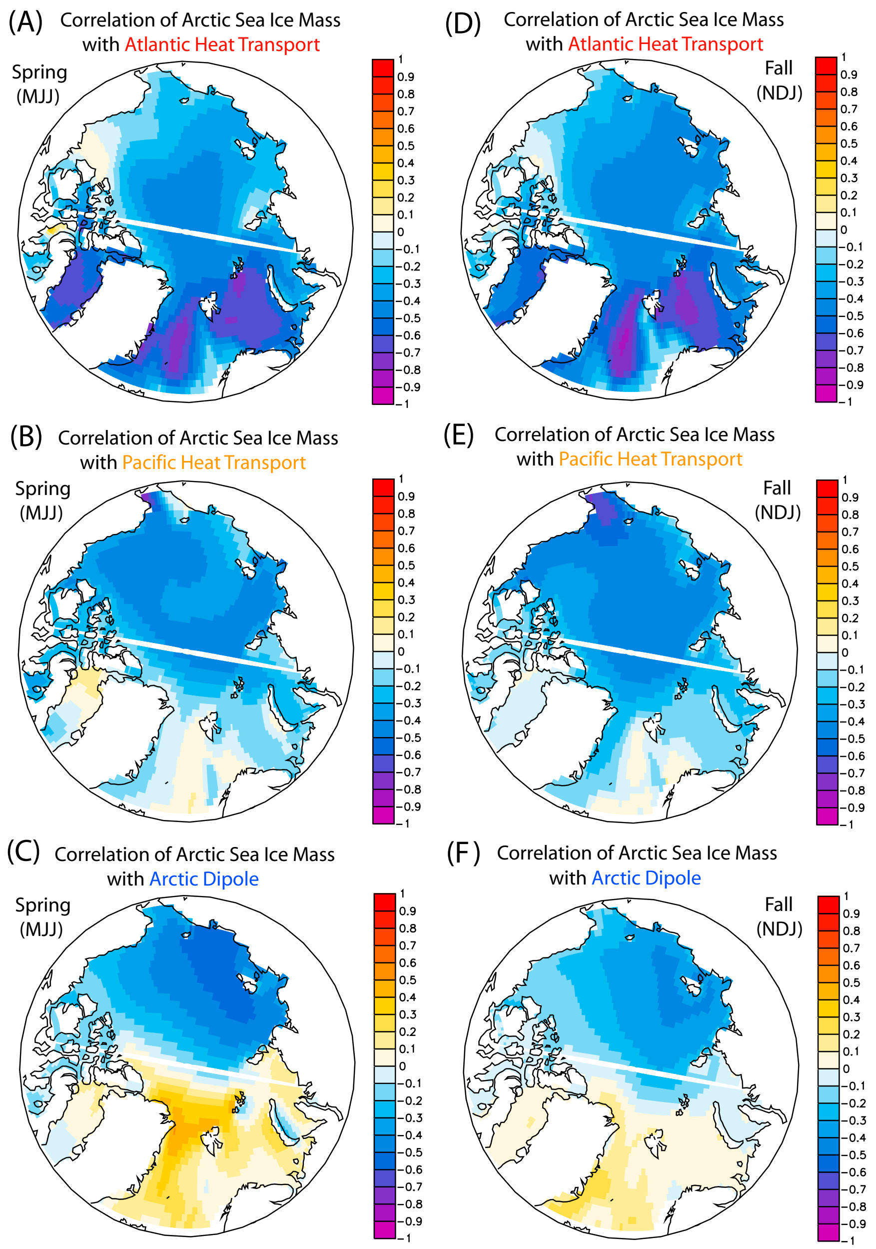

Fig. S4. Correlation maps between LF Arctic sea ice mass anomalies (kilogram per square meter) and each of the three LF predictors in CM2.1 at spring [May–July (MJJ)] (*A*–*C*) and fall [November–January (NDJ)] (*D*–*F*), respectively. (*A* and *D*) Correlations with anomalous HT_{ATL} (2-y lead). (*B* and *E*) Correlations with anomalous HT_{PAC} (2-y lead). (*C* and *F*) Correlations with anomalous AD (1-y lead).

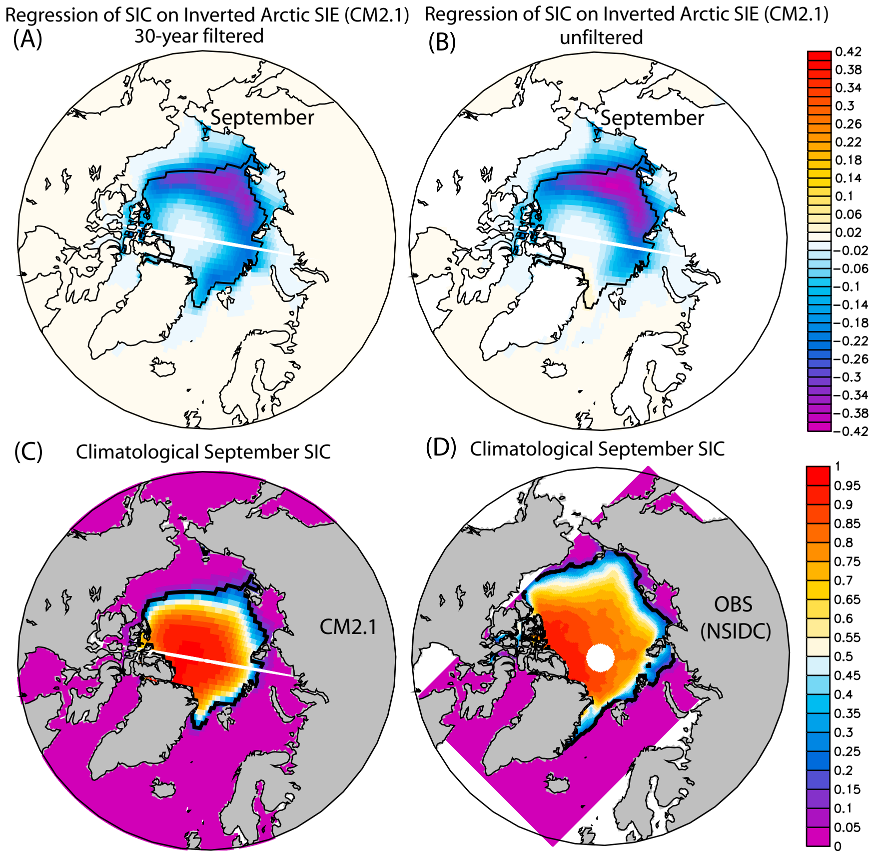

Fig. S5. Comparison of 30-y LF and unfiltered patterns of September Arctic SIC anomalies, and comparison of simulated and observed climatological September SIC. (*A*) Regression of LF anomalous September SIC on 1 million km^2 LF inverted September Arctic SIE anomaly from CM2.1 (*B*) Regression of unfiltered anomalous September SIC on 1 million km^2 unfiltered inverted September Arctic SIE anomaly from CM2.1. The spatial patterns in *A* and *B* are similar except the LF anomalies in *A* are larger in the Atlantic side and smaller in the Pacific side than those unfiltered anomalies in *B*. (*C*) Simulated climatological September SIC from CM2.1. (*D*) Observed climatological September SIC over 1979–2013 (NSIDC data). The thick black lines mark the positions of climatological September ice edge where climatological September SIC drops below 15%.

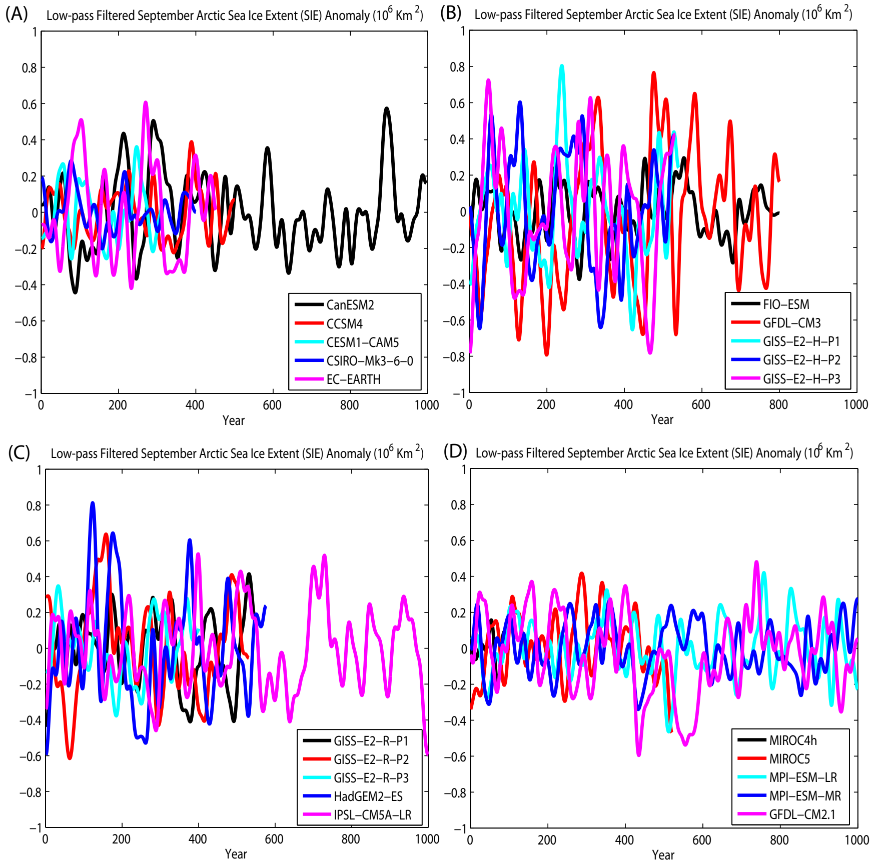

Fig. S6. September Arctic SIE anomalies (30-y LF) in 19 CMIP5 preindustrial control simulations and in the last 1,000 y from the 3,600-y segment of GFDL CM2.1 control simulation. (*A*) CMIP5 models 1–5. (*B*) CMIP5 models 6–10. (*C*) CMIP5 models 11–15. (*D*) CMIP5 models 16–19 and GFDL CM2.1. The segments of control simulations with the long-term drifts in September Arctic SIE are not included. The CMIP5 data are downloaded from CMIP5 archive produced and made available by the World Climate Research Programme Working Group on Coupled Modeling, which is responsible for CMIP, and by the climate modeling groups. For CMIP, the US Department of Energy's Program for Climate Model Diagnosis and Intercomparison provides coordinating support and led development of software infrastructure in partnership with the Global Organization for Earth System Science Portals.

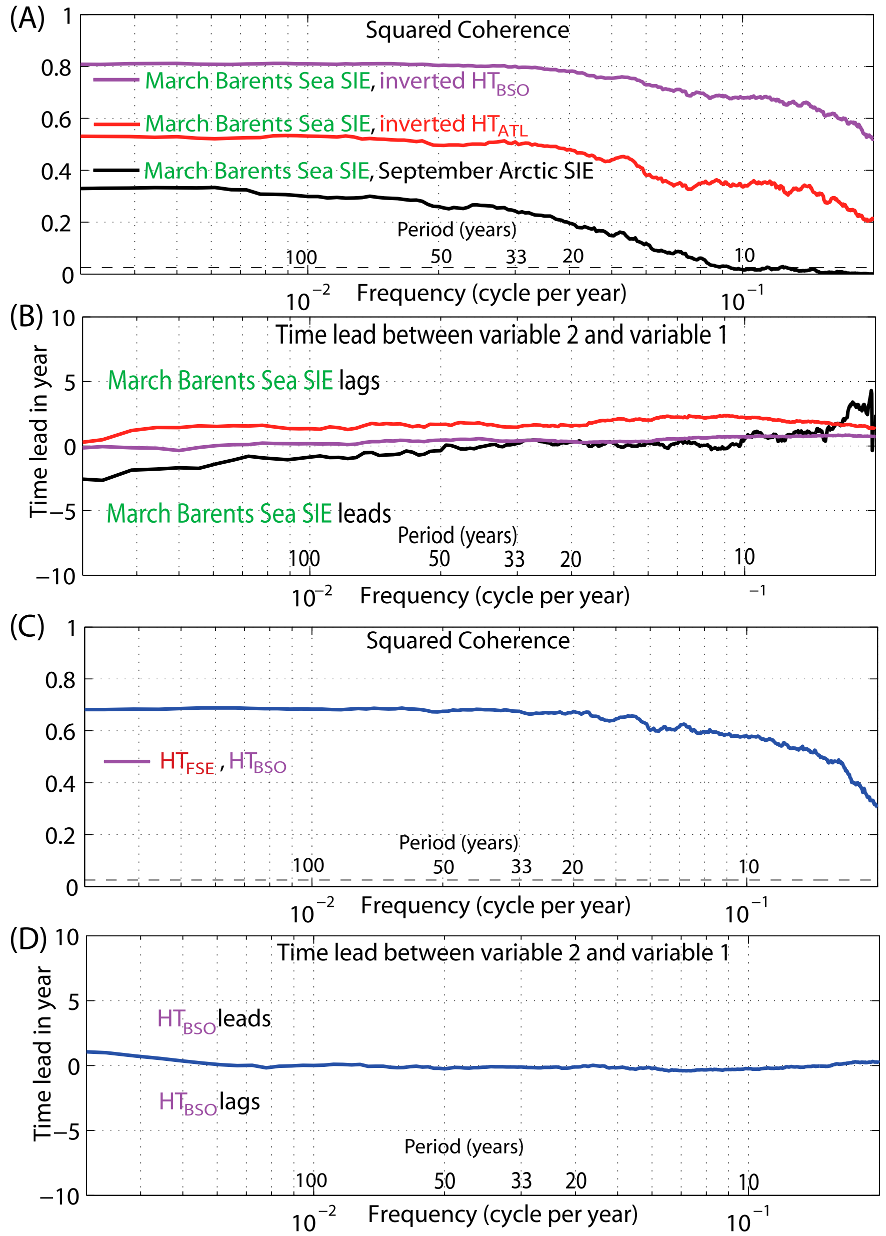

Fig. S7. Cross-spectral analysis from CM2.1. (*A* and *B*) Squared coherence (*A*) and time lead in years (*B*) among unfiltered variables (March Barents Sea SIE anomalies vs. inverted HT_{ATL} and HT_{BSO} anomalies, and vs. September Arctic SIE anomalies). (*C* and *D*) Squared coherence (*C*) and time lead in years (*D*) among unfiltered HT_{BSO} and HT_{FSE} anomalies. The dashed black lines in *A* and *C* are the 99% significance levels.

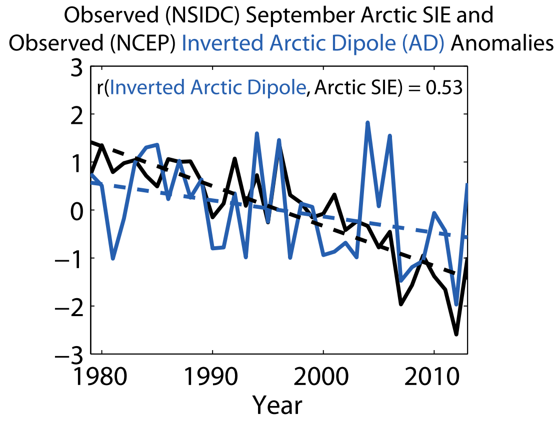

Fig. S8. Observed inverted Arctic Dipole (NCEP/NCAR reanalysis, blue line) and September Arctic SIE (NSIDC, black line) anomalies from 1979 to 2013 (normalized by their SDs, 31.7 hPa and 1.1 million km^2, respectively). The dashed lines are the corresponding trends over the same period.

Table S1. September Arctic SIE (climatological mean and SD of 30-y LF anomaly) in 19 CMIP5 preindustrial control simulations and in the 3,600-y segment of GFDL CM2.1 preindustrial control simulation

Model list	Mean, million km^2	SD (30-y LF), million km^2	Length of control simulation, years
CanESM2	5.1	0.21	996
CCSM4	9.0	0.14	501
CESM1-CAM5	8.0	0.16	319
CSIRO-Mk3-6–0	11.6	0.10	400
EC-EARTH	10.0	0.26	452
FIO-ESM	7.8	0.13	800
GFDL-CM3	5.3	0.36	800
GISS-E2-H-P1	8.0	0.26	540
GISS-E2-H-P2	7.3	0.31	531
GISS-E2-H-P3	5.7	0.34	531
GISS-E2-R-P1	7.2	0.20	550
GISS-E2-R-P2	7.0	0.27	531
GISS-E2-R-P3	6.4	0.17	400
HadGEM2-ES	6.0	0.30	576
IPSL-CM5A-LR	9.0	0.22	1,000
MIROC4h	5.8	0.08	100
MIROC5	8.4	0.17	521
MPI-ESM-LR	8.2	0.15	1,000
MPI-ESM-MP	8.0	0.14	1,000
GFDL-CM2.1	4.5	0.22	3,600

The segments of control simulations with long-term drifts in September Arctic SIE are not included.

Table S2. Simulated simple regression coefficients between September Arctic SIE and other variables, and the estimated contributions to the observed decline trend in September Arctic SIE

Related variables	Simple regression coefficients	Estimated contributions to September Arctic SIE decline trend
35-y trends of September Arctic SIE and HT_{BSO}	-0.039×10^6 km^2/TW	0.33×10^6 km^2/decade (1979–2013)
35-y trends of September Arctic SIE and AD	-0.01×10^6 km^2/hPa	0.11×10^6 km^2/decade (1979–2013)
11-y trends of September Arctic SIE and HT_{PAC}	-0.21×10^6 km^2/TW	0.84×10^6 km^2/decade (2001–2011)